J Biomol NMR (2014) 58:113–122
DOI 10.1007/s10858-013-9809-8

ARTICLE

A probe to monitor performance of ^{15}N longitudinal relaxation experiments for proteins in solution

Rieko Ishima

Received: 15 July 2013 / Accepted: 24 December 2013 / Published online: 5 January 2014

Abstract The magnitude of the ^{15}N longitudinal relaxation rate typically decreases as magnetic field strength increases in globular proteins in solution. Thus, it is important to test the performance of ^{15}N longitudinal relaxation experiments at high field strength. Herein, a tool to investigate systematic errors in ^{15}N longitudinal relaxation rate, R_1, is introduced. The tool, a difference in R_1 values between the two components of the ^{1}H-coupled ^{15}N magnetizations, $R_1^{(1)}$–$R_1^{(2)}$, conveniently detects inefficiencies in cancellation of cross correlation between ^{1}H–^{15}N dipolar coupling and ^{15}N chemical shift anisotropy. Experiments, in varying conditions, and simulations of a two-spin system indicate that insufficient cancellation of the cross correlation is due to (1) ^{1}H pulse imperfection and (2) ^{1}H off-resonance effect, and (3) is further amplified by residual ^{15}N transverse magnetization that is caused by the ^{15}N off-resonance effect. Results also show that this problem can be easily and practically remedied by discarding the initial decay points when recording ^{15}N longitudinal relaxation in proteins.

Keywords NMR · Backbone dynamics · Longitudinal · Relaxation · T_1 · Protein

Electronic supplementary material The online version of this article (doi:10.1007/s10858-013-9809-8) contains supplementary material, which is available to authorized users.

R. Ishima (✉)
Department of Structural Biology, University of Pittsburgh School of Medicine, Biomedical Science Tower 3, 3501 Fifth Avenue, Pittsburgh, PA 15260, USA
e-mail: ishima@pitt.edu

Introduction

Experiments to determine ^{15}N longitudinal relaxation rate (R_1) and ^{15}N transverse relaxation rate (R_2) along with {^{1}H}–^{15}N NOE for proteins in solution were mainly developed in the 1990s when 500 or 600 MHz NMR instruments were commonly available (Grzesiek and Bax 1993; Kay et al. 1989; Palmer et al. 1992; Peng et al. 1991; Schneider et al. 1992; Skelton et al. 1993). Protein backbone dynamics are often evaluated using these relaxation parameters, either directly or through a generalized order parameter that is calculated based on the relaxation parameters (Andrec et al. 1999; Bruschweiler 2003; Campbell et al. 2000; Chen et al. 2004; Clore et al. 1990; d'Auvergne and Gooley 2003, 2006; Dayie et al. 1996; Fushman and Cowburn 2001; Fushman et al. 1999; Idiyatullin et al. 2003; Igumenova et al. 2006; Ishima and Torchia 2000; Jarymowycz and Stone 2006; Kay 2005; Kay et al. 1989; Korchuganov et al. 2004; Kroenke et al. 1998; Lee and Wand 1999; Lee et al. 1997; Lipari and Szabo 1982a, b; Mandel et al. 1995; Nirmala and Wagner 1988; Orekhov et al. 1994; Palmer 2001; Palmer et al. 1991; Pelupessy et al. 2003; Redfield 2004; Schneider et al. 1992; Spyracopoulos 2006; Tjandra et al. 1995). Since relaxation rates depend on the magnetic field strength, as well as the relaxation mechanism and protein dynamics, it is necessary to optimize and validate relaxation experiments and their analysis under a wide variety of conditions, including a range of magnetic field strengths.

In experiments that measure longitudinal relaxation, such as ^{15}N R_1 and {^{1}H}–^{15}N NOE, the relative systematic error may become pronounced as the magnetic field strength increases, because the magnitudes of the spectral density functions, $J(\omega_N)$ and $J(\omega_H)$, at ^{15}N and ^{1}H resonance angular frequencies, respectively, are reduced. When

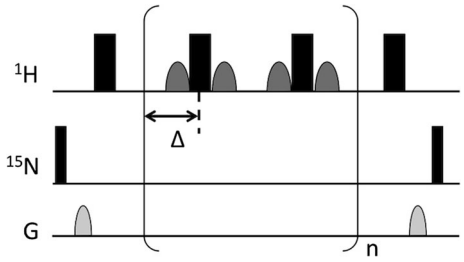

Fig. 1 Pulse scheme during the relaxation period of a ^{15}N R_1 experiment, having in-phase ^{15}N magnetization at the start of the scheme. *Thick and thin rectangular bars* indicate 180° and 90° pulses, respectively. *Gray* sine-bell ^{1}H dimension indicates shaped pulse for water signal flip back. "G" indicates pulse-field gradient (PFG). Δ is a half delay from a center of a ^{1}H 180° pulse to the next one. Note that both sequences were carried out with or without the water excitation pulses for the initial test (see the text). To distinguish the relaxation delay between the number of scans for accumulation, *d1*, the delay for R_1 experiment is noted as T_{R1} (=4nΔ) in this manuscript

applied to proteins with a rotational correlation time, τ_R, that satisfies a large molecular condition, $\tau_R\omega_N \gg 1$, {^{1}H}–^{15}N NOE is well known to become insensitive as a function of the magnetic field strength, due to a reduction in the ^{1}H–^{15}N dipolar coupling (DD) term of the spectral density function at the ^{15}N and ^{1}H resonance frequencies, ω_N and ω_H, respectively (Ferrage et al. 2008, 2009; Gong and Ishima 2007; Renner et al. 2002). Despite the increase in the ^{15}N chemical shift anisotropy (CSA) as a function of the magnetic field strength, the total ^{15}N R_1 decreases in a globular protein as τ_R increases (when $\tau_R\omega_N \gg 1$). This is primarily because ω_N dependence in the CSA cancels the ω_N dependence in the spectral density function (when $\tau_R\omega_N \gg 1$), in contrast to the case in small molecules. While errors in R_1 measurements introduced by amide-proton exchange and water proton spin saturation have been addressed (Chen and Tjandra 2012; Grzesiek and Bax 1993), other errors in the ^{15}N R_1 measurements have not been well studied.

In addition to the water-amide exchange effect, performance of ^{15}N R_1 experiment may be affected by how well the cross correlation effect between ^{1}H–^{15}N DD and ^{15}N CSA is cancelled with ^{1}H 180° pulses during the R_1 delay (Fig. 1) (Boyd et al. 1990; Kay et al. 1992; Palmer et al. 1992; Peng et al. 1991). When ^{1}H 180° pulses are *not* employed during the R_1 delay period, the two components of the ^{1}H–^{15}N J-coupled ^{15}N magnetization relax differently. The ^{15}N R_1 experiment is performed with ^{1}H 180° pulses during the R_1 delay to cancel the cross correlation effect (Fig. 1) (Goldman 1984). Although it is optimal to sample the time point at $\sim 1/R_1$ for a data set that exhibits a single-exponential decay function, according to the sampling theory (Jones 1997; Jones et al. 1996), typically multiple R_1 delay points are recorded to verify a single-exponential decay, i.e., to ensure cancellation of the DD-CSA cross correlation (Chen and Tjandra 2012; Farrow et al. 1994; Mandel et al. 1995) and because variation in the R_1 values is expected.

Herein, to investigate the performance of ^{15}N R_1 experiments, a difference in R_1 values between the two components of the ^{1}H-coupled ^{15}N magnetizations, $R_1^{(1)}$–$R_1^{(2)}$, was introduced as a tool to monitor a residual of the cancellation of the DD and CSA cross-correlation in ^{15}N R_1 experiments. Analysis shows the DD-CSA cross correlation is not sufficiently suppressed in the initial decay at a 900 MHz NMR instrument, due to ^{1}H pulse imperfection and ^{1}H off-resonance effect, and further amplified by residual ^{15}N transverse magnetization. In contrast, such error was not observed at 600 MHz, a frequency at which, compared to 900 MHz, the experiment has a lower signal-to-noise ratio and a smaller CSA effect. To avoid this contamination, discarding the initial decay of ^{15}N R_1 experiments is recommended.

Materials and methods

NMR experiments

^{15}N longitudinal relaxation experiments were conducted at 20° on Bruker Avance 600 and 900 NMR instruments with 60.828 and 91.22 MHz ^{15}N resonance frequencies, respectively, using 0.8 mM ^{15}N labeled perdeuterated ubiquitin at pH 4.5, purchased and prepared as described previously (Myint et al. 2009). Three ^{15}N R_1 experiments (I, II, and III) were recorded without a ^{1}H 180° pulse during the t_1 evolution, to allow a pair of J-coupled ^{15}N peaks to be observed (Fig. 1, supplement material): experiments (I) and (II) were performed on a 900 MHz instrument, with ^{1}H 180° pulses, to suppress DD-CSA cross-correlation (Kay et al. 1992; Palmer et al. 1992), applied with $\Delta = 6.25$ ms [experiment (I)] or $\Delta = 12.5$ ms [experiment (II)]. Experiment (III) was performed on a 600 MHz instrument with the same parameters as experiment (I), $\Delta = 6.25$ ms. In all experiments, ^{1}H 90° and ^{15}N 90° pulses were set to ~10 and ~46 μs, and the delays applied for the longitudinal relaxation measurements, T_{R1}, were: 0, 0.05, 0.1, 0.15, 0.2, 0.3, 0.4, 0.5, 0.8, and 1.0 s. A total of 8 scans were accumulated with a recycle delay (d1) = 4 s. ^{1}H water flip back pulses were inserted after the first INEPT period and during the R_1 delay, prior and subsequent to the ^{1}H 180° pulses that suppress DD-CSA cross-correlation (Fig. 1). In all ^{15}N longitudinal relaxation experiments here, the Freeman Hill phase cycle (+Z and −Z magnetization time courses are accumulated) that has been implemented to standard biomolecular ^{15}N longitudinal relaxation experiments was applied (Freeman and Hill 1971).

In each experiment, (I), (II), and (III), R_1 values were determined by assuming a single exponential decay function, using (a) the entire 10 data points, (b) the initial 6 points (0–0.3 s), and (c) the last 6 points (0.2–1.0 s). For each R_1 fit, the initial intensity, I^{fit}, was optimized along with R_1. Uncertainties in the optimized R_1 and I^{fit} were determined by Monte-Carlo error estimation, by generating a hundred sets of synthetic intensity data, to allow a Gaussian distribution with the ideal intensities as the mean (Nicholson et al. 1992).

Data were evaluated by correlating R_1 values determined using (a) the entire 10 data points with those determined from (b) the initial 6 points (0–0.3 s) or (c) the last 6 points (0.2–1.0 s). Further, the R_1 difference of a pair of J-coupled ^{15}N resonances, $R_1^{(1)}$–$R_1^{(2)}$, were plotted as a function of off-resonance frequency, which is the difference between the signals and the carrier frequency. For the latter, the carrier frequency of the ^{15}N spectrum was set at 117 ppm for the 900 MHz experiment or 122 ppm, for the 600 MHz experiments. The carrier frequency was shifted for the 600 MHz experiments to detect signals far from the carrier frequency.

Simulations

To estimate the mechanism of the errors in the ^{15}N longitudinal relaxation experiments, the time course of magnetization was calculated for a scalar-coupled two-spin system, ^1H–^{15}N, with an additional proton sink, using the formula that was described previously (Allard et al. 1998; Myint et al. 2009). Here, simulations were performed by assuming the following parameters: a single rotational correlation time, 4.6 ns; magnetic field strength, 21.14 T (91.25 and 900.14 MHz resonance frequencies for ^{15}N and ^1H, respectively); ^{15}N CSA, 170 ppm; N–H distance, 1.02 Å; additional ^1H R_1 from surrounding protons, 2 s^{-1}; additional ^1H R_2 from surrounding protons, 20 s^{-1}; additional $2N_ZH_Z$ term from surrounding protons, 2 s^{-1}; Δ, 6.25 ms; ^1H and ^{15}N 90° pulses, ~10 and ~46 μs, respectively. Simulation results were stored at the end of every 25 ms (=4Δ) cycle. Simulations were performed at ^1H carrier frequencies of 3,000 and 400 Hz (3.3 and 0.44 ppm, respectively), assuming a correct ^{15}N B_1 field strength at the start of Z-relaxation and a 10 % error in the ^1H B_1 field strength. In the latter, a relatively large B_1 calibration error was assumed for presentation purposes.

Simulation results were analyzed in two ways: (1) extracting the time course of various components of the magnetization, such as $N_Z \pm 2N_ZH_Z$, $2N_ZH_Z$, N_X, and N_Y, from T_{R1} = 0–1 s at a 1,000 Hz ^{15}N off-resonance frequency (defined as a signal position from the carrier frequency), and (2) extracting intensities at T_{R1} = 0.1 s as a function of ^{15}N off-resonance frequency from 0 to 1,800 Hz. In all the simulations, the initial condition at which ^{15}N and ^1H nuclei were located in the −Y and Z directions, respectively, was employed. A set of two time courses were all calculated with the ^{15}N 90° pulse either at +X or −X phases for the Freeman–Hill cycle (which brings the up and down magnetization to +Z and −Z starting, respectively) (Freeman and Hill 1971). Thus, this simulation contains the effect of ^{15}N off-resonance frequency during the initial 90° pulse. All the simulations were done using the MATLAB software (The Mathworks Inc., Natick, MA).

Results and discussion

An aim of this study was to investigate the performance of the ^{15}N R_1 experiment at high magnetic field strength, 900 MHz, where the R_1 magnitude is small, compared to that at lower field strengths, in a globular protein ($\tau_R\omega_N \gg 1$), thus making it more sensitive to systematic errors. The performance of the actual ^{15}N R_1 experiments was first evaluated taking into account the effect of water magnetization recovery. As recently described by Tjandra's group, when water-flip back pulses (sine-shaped pulses in Fig. 1) are not applied during T_{R1}, R_1 values determined with a short recycle delay ($d1$ = 2 s) are not consistent with those determined with a long delay ($d1$ = 4 s) (Figure S1A) (Chen and Tjandra 2012). In contrast, when water-flip back pulses are applied, R_1 values are consistent regardless of the delay, because water proton spin saturation is suppressed (Figure S1B) (Chen and Tjandra 2012). Thus, in all measurements to be described, ^{15}N R_1 values were recorded with the water-flip back pulses at $d1$ = 4 s. Note that the systematic errors shown below were observed even when R_1 was recorded with the water-flip back pulses at $d1$ = 4 s (Figure S1C).

Errors in the initial decay of magnetization in ^{15}N R_1

At 900 MHz, although the ^{15}N R_1 values recorded with a 2 s recycle delay (with water-flip back pulses applied during the T_{R1} period) were almost identical to those recorded with a 4 s delay, as described previously (Chen and Tjandra 2012) and tested here (Figure S1), ^{15}N R_1 rates determined using the initial 6 points (0–0.3 s points) were significantly different from those determined using the entire data set (10 points) (Fig. 2a). On the other hand, when ^{15}N R_1 rates determined using the last 6 points (those sampled beyond the initial decay of magnetization) were compared with those determined using the entire data set, a significant increase in the correlation coefficient, R, was observed (from 0.915 to 0.974) (compare Fig. 2a, b). The Δ value had no effect on this observation, as a similar

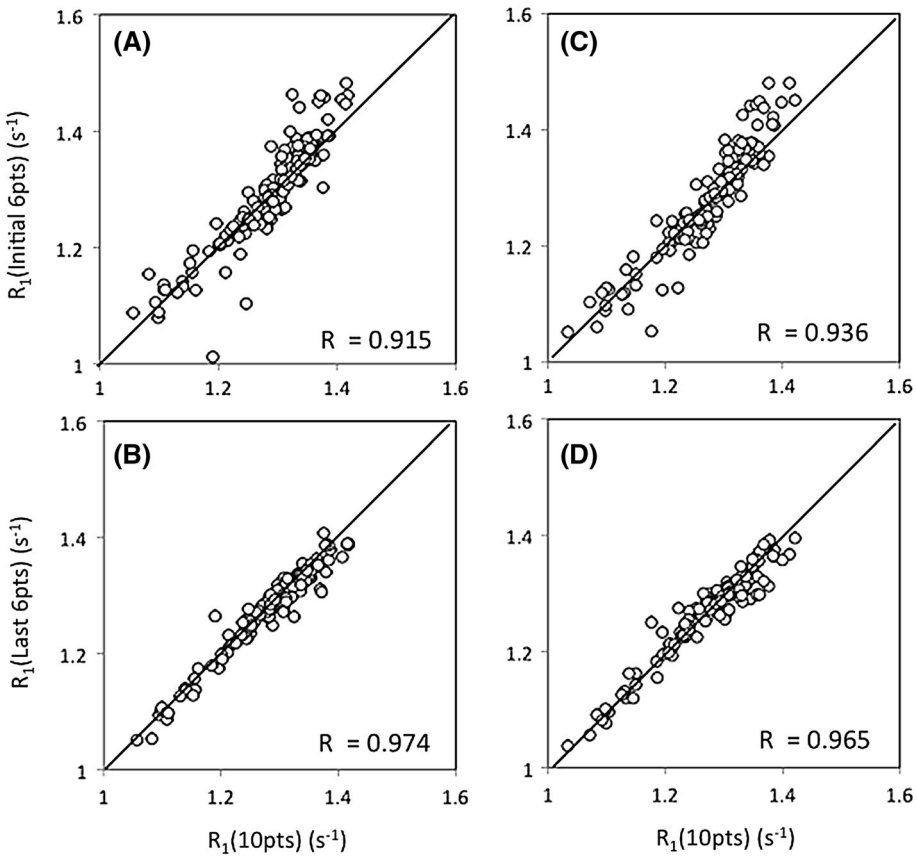

Fig. 2 Comparison of ^{15}N R_1 rates determined using **a**, **c** the initial 6 points or **b**, **d** the last 6 points to those determined using all 10 points. The data were obtained using pulse sequences with **a**, **b** $\Delta = 6.25$ ms or **c**, **d** $\Delta = 12.5$ ms and with water flip back pulses (Fig. 1). R indicates the correlation coefficient of each comparison. The 10 point R_1 rates, obtained using $\Delta = 6.25$ ms and $\Delta = 12.5$ ms, showed a correlation of 0.99. Data were recorded at 91.22 MHz ^{15}N resonance frequency

improvement in the correlation coefficient, from 0.936 to 0.965 (Fig. 2c, d), was observed for ^{15}N R_1 recorded using $\Delta = 12.5$ ms. In both conditions, removing data acquired with short delay times improved the correlation coefficient.

To obtain insight into the behavior of the observed longitudinal magnetization decay, $R_1^{(1)}$–$R_1^{(2)}$ was plotted as a function of the off-resonance frequency for the entire data set (10 points), the initial 6 data points (0–0.3 s points), or the last 6 data points (0.2–1.0 s points) (Fig. 3). For R_1 determined using the entire data set, $R_1^{(1)}$–$R_1^{(2)}$ was small for signals located at less than 1,000 Hz ^{15}N off-resonance but was large for those signals at more than 1,000 Hz ^{15}N off-resonance (Fig. 3a). In addition, the $R_1^{(1)}$–$R_1^{(2)}$ values for the initial 6 points were relatively high, with substantial sinusoidal modulation even close to the ^{15}N carrier frequency (Fig. 3b). These modulations introduce an error of ca. 10 % in R_1, which is significantly larger than the uncertainty calculated based on signal-to-noise ratio (average fractional error in R_1, 1.9 %, Table 1). In fact, the plots of $R_1^{(1)}$–$R_1^{(2)}$ determined using the last 6 points (0.3–1.0 s) show that $R_1^{(1)}$–$R_1^{(2)}$ is negligible over the entire range of off-resonance frequencies, even for those above 1,000 Hz (Fig. 3c): the correlation coefficient of the R_1 values obtained using the initial 6 points with those obtained using the entire data set improves from 0.915 to 0.964 upon eliminating the signals at >500 Hz ^{15}N off-resonance (Table 1). A similar tendency was observed for the data set recorded with $\Delta = 12.5$ ms (Fig. 3d, f): the correlation coefficient in Fig. 2c increased from 0.936 to 0.966 even when signals >500 Hz off-resonance were eliminated from the comparison of the R_1 values (Table 1). These data indicate that the DD-CSA cancellation was insufficient for data points recorded with short delay times.

Effect of Δ in the ^{15}N R_1 experiments

When DD-CSA cancellation is insufficient, it has a significant impact on the Δ-dependence of the cross correlation cancellation efficiency, where Δ is the duration between the two ^{1}H 180° pulses (Fig. 1). However, comparisons of ^{15}N R_1 values that were determined using $\Delta = 6.25$ ms (Figs. 2a, b and 3a–c) with those using 12.5 ms did not exhibit significant differences (Figs. 2c, d and 3d–f). Fractional errors in R_1 were only slightly larger in ^{15}N R_1 values obtained using $\Delta = 6.25$ ms than those using 12.5 ms (Table 1). To better understand small errors in R_1 values, R_1 errors that resulted from deviations between data and fits assuming a single-exponential model were compared instead of R_1 values themselves (Fig. 4). As expected, for the data recorded using $\Delta = 6.25$ ms, R_1 errors for those determined using the initial 6 points (0–0.3 s) were larger than those determined using the entire

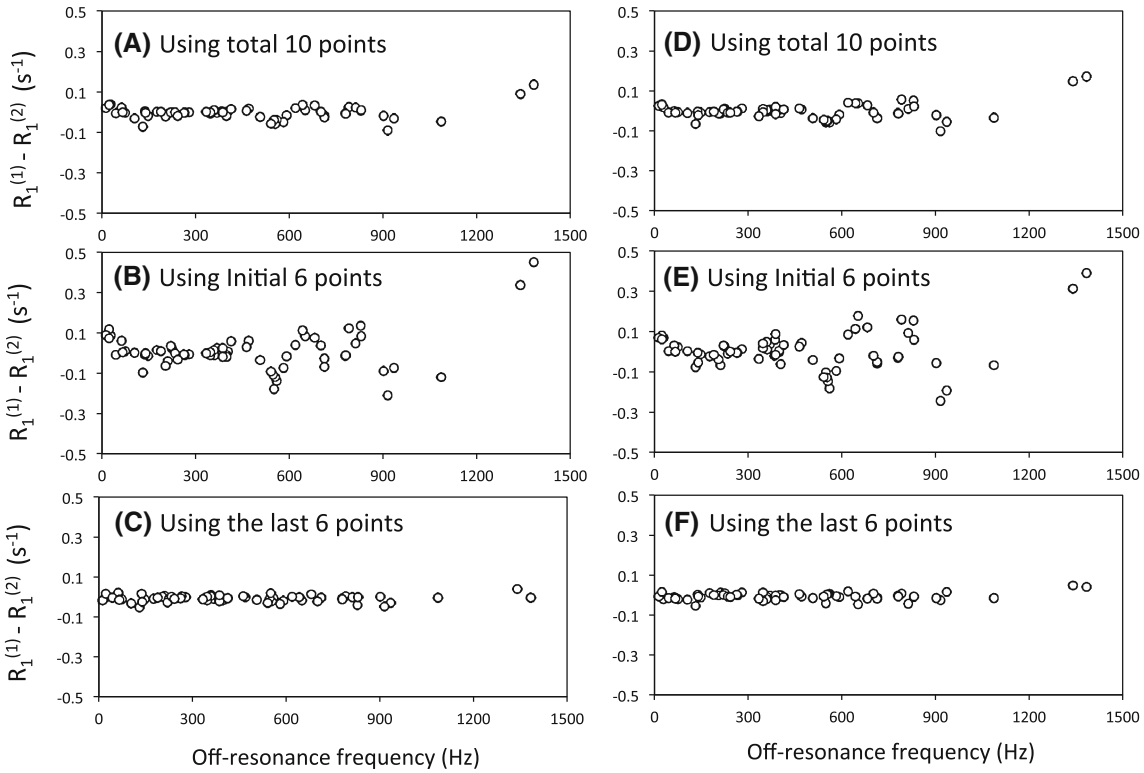

Fig. 3 ^{15}N $R_1^{(1)}$–$R_1^{(2)}$, obtained from the R_1 data in Fig. 2, shown as a function of ^{15}N off-resonance frequency (defined here as a signal position from the carrier frequency) for those determined using **a**, **d** the entire 10 points, **b**, **e** the initial 6 points, or **c**, **f** the last 6 points. The data were obtained using pulse sequences with **a**–**c** $\Delta = 6.25$ ms and **d**–**f** $\Delta = 12.5$ ms

Table 1 Fractional error in R_1 and correlation to the 10 point fits

Data points used to determine R_1 values	900 MHz						600 MHz		
	$\Delta = 6.25$ ms (experiment I)			$\Delta = 12.5$ ms (experiment II)			$\Delta = 6.25$ ms (experiment III)		
	Average R_1 (s^{-1})	Average R_1 fractional error (%)	Correlation coefficient of R_1^a	Average R_1 (s^{-1})	Average R_1 fractional error (%)	Correlation coefficient of R_1^a	Average R_1 (s^{-1})	Average R_1 fractional error (%)	Correlation coefficient of R_1^a
Entire 10 points (0–1.0 s)	1.28	1.2	–	1.28	1.1	–	1.76	1.6	–
Initial 6 points (0–0.2 s)	1.29	1.9	0.915 (0.964)	1.28	1.6	0.936 (0.966)	1.70	3.0	0.975 (0.978)
Last 6 points (0.3–1.0 s)	1.28	1.1	0.974 (0.982)	1.27	1.1	0.965 (0.984)	1.80	1.7	0.980 (0.983)

[a] Correlation coefficients of R_1 values calculated using a subset of data points relative to those determined using the entire dataset (10 points). Correlation coefficients in parenthesis were calculated for the signals that are located within 500 Hz of the carrier frequency

10 data points (0–1.0 s) (Fig. 4a), whereas R_1 errors for those determined using the last 6 points (0.2–1.0 s) were significantly smaller than those determined using the entire 10 data points (0–1.0 s) (Fig. 4b). Although a similar tendency was observed for the datasets recorded using $\Delta = 12.5$ ms, the overall R_1 errors were clearly smaller than in the case of $\Delta = 6.25$ ms. This observation of better performance of a large Δ is consistent to the previous results in off-resonance $R_{1\rho}$ experiments, in which application of infrequent ^1H 180° pulses resulted in more efficient DD-CSA cancellation than frequent application of ^1H 180° pulses (Korzhnev et al. 2002; Massi et al. 2004). Observation of similar improvement of the performance of the R_1 experiments by increasing Δ also supports that the observed ^{15}N R_1 error is related to the application of ^1H 180° pulses.

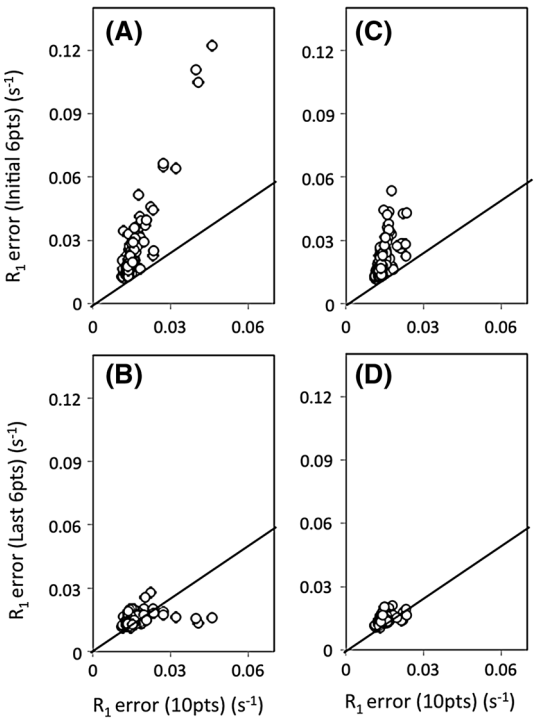

Fig. 4 Comparison of ^{15}N R_1 errors for R_1s determined using **a**, **c** the initial 6 points or **b**, **d** the last 6 points, with the errors for R_1s determined using the entire 10 points. The data were obtained using pulse sequences with **a**, **b** $\Delta = 6.25$ ms or **c**, **d** $\Delta = 12.5$ ms, both containing water flip back pulses (Fig. 1). These R_1 errors were obtained for the R_1 data shown in Fig. 2

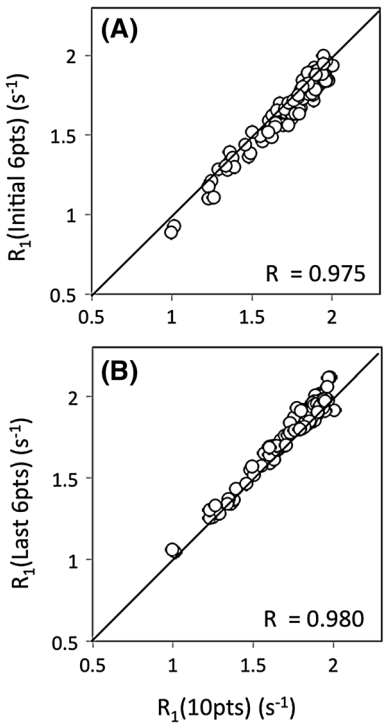

Fig. 5 Comparison of ^{15}N R_1 rates determined using **a** the initial 6 points or **b** the last 6 points with those determined using the entire 10 points. The data were obtained using pulse sequences with $\Delta = 6.25$ ms, containing water flip back pulses (Fig. 1). Data were recorded at 60.83 MHz ^{15}N resonance frequency

Pronounced initial-decay errors at high static-magnetic field strength

When the R_1 experiments (using $\Delta = 6.25$ ms) were performed at 600 MHz, significant differences between R_1 values measured using the initial decay and the entire decay were not observed. ^{15}N R_1 values that were determined using the initial 6 points (0–0.3 s) showed a high correlation, $R = 0.975$, with those determined using the entire 10 points (0–1.0 s) (Fig. 5a). Even for the signals that are located within 500 Hz from the carrier frequency, R was increased only to 0.978 (Table 1). These correlation coefficients were, in fact, similar to those obtained using the last 6 points (0.2–1.0 s), $R = 0.980$ (Fig. 5b). Although $R_1^{(1)}$–$R_1^{(2)}$ for those determined using the initial 6 points is slightly more noisy than those determined using the last 6 points, significant sinusoidal modulation of $R_1^{(1)}$–$R_1^{(2)}$ was not observed (Fig. 6). The average fractional error at 600 MHz was 1.6 % for R_1 values determined using the entire data set and was only slightly higher than that at 900 MHz (Table 1). Thus, the observed sinusoidal modulation of $R_1^{(1)}$–$R_1^{(2)}$ at 900 MHz (>10 % changes in R_1 values) but not at 600 MHz is not likely due to the signal-to-noise difference of data recorded at the two magnetic field strengths.

Factors that contribute to the error in the initial magnetization decay

The above data consistently indicate that the DD-CSA cancellation was insufficient at the initial magnetization decay in the ^{15}N R_1 experiment. This error likely relates to contamination of the transverse magnetization, due to significant ^{15}N off-resonance dependence. However, it is surprising that such a ^{15}N off-resonance dependence, caused by chemical shift precession, affects substantial $R_1^{(1)}$–$R_1^{(2)}$ difference. Indeed, when only the last 6 points (0.3–1.0 s) were used for the analysis, $R_1^{(1)}$–$R_1^{(2)}$ became negligible *over the entire range* of off-resonance frequencies (Fig. 3). The frequency range, in which the sinusoidal modulation of $R_1^{(1)}$–$R_1^{(2)}$ could be primarily ignored, was below 500 Hz off-resonance (Fig. 3) and was much smaller than the range not affected by off-resonance effects of ^{15}N R_2 (Myint et al. 2009). These observations imply that the ^{15}N off-resonance effect may not be the only cause of the residual $R_1^{(1)}$–$R_1^{(2)}$. Thus, to investigate the mechanism of the residual of $R_1^{(1)}$–$R_1^{(2)}$, simulation of bulk magnetization was performed.

The simulated time-course was plotted at each 25 ms (=4Δ) interval, with the expectation that the cross correlation at each data point in the plot would be cancelled.

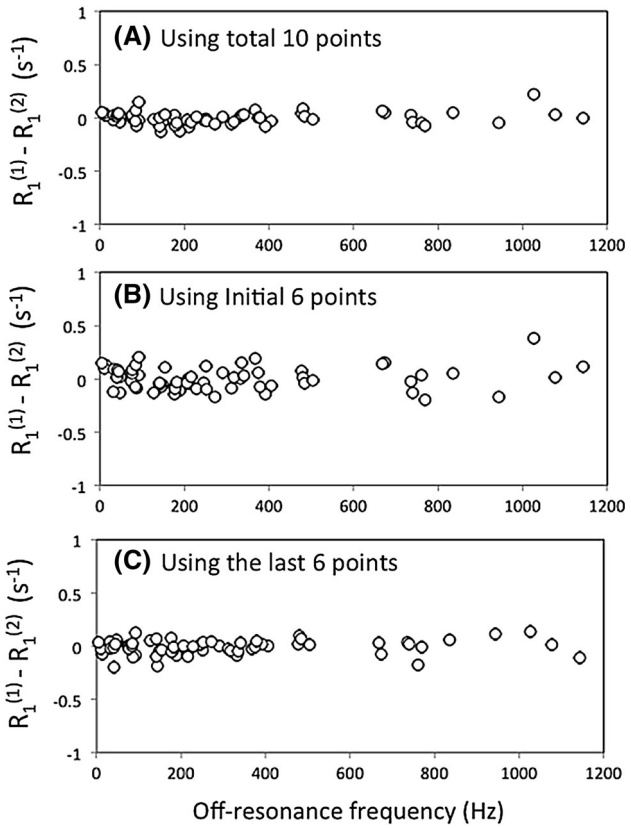

Fig. 6 ^{15}N $R_1^{(1)}$–$R_1^{(2)}$, obtained from the R_1 data in Fig. 5, shown as a function of off-resonance frequency for those determined using **a** the entire 10 points, **b** the initial 6 points, or **c** the last 6 points

Nevertheless, differences in the initial longitudinal magnetization decay of a pair of ^1H–^{15}N J-coupled ^{15}N peaks were observed in both Freeman-Hill phases (Fig. 7a, b). The difference in the longitudinal magnetization of the two components was also directly shown as a $2N_ZH_Z$ term in Fig. 7c. The decay time is qualitatively consistent to the known $2N_ZH_Z$ relaxation time of proteins in solution (Boyd et al. 1990; Kay et al. 1992; Palmer et al. 1992; Peng et al. 1991). Although the average of the two components cancel out the cross correlation effects in an isolated-two spin system, this is known not to be the case in proteins (Kay et al. 1992; Palmer et al. 1992). Thus, the difference in the initial longitudinal magnetization decay of the two components is expected to remain, resulting in the difference between $R_1^{(1)}$ and $R_1^{(2)}$. This difference in the two components did not linearly depend on the ^1H off-resonance frequency and even 400 Hz off-resonance impacts the difference in the two ^{15}N components (Fig. 7d, f). Importantly, this difference was *not* observed when a correct ^1H radio-frequency pulse was employed, indicating that the imperfection of ^1H 180° pulse caused the intensity difference between the two J-coupled ^{15}N peaks.

The plot of the time course of residual ^{15}N transverse magnetization shows that the intensity varies as a function of ^{15}N off-resonance frequency with a sinusoidal modulation (dashed lines in Fig. 7c, f). Note, since the actual experiment was done with a pulse field gradient after the initial inversion pulse, this simulation may over estimate the effects of the ^{15}N transverse magnetization. Nevertheless, the sinusoidal modulation, 1–2 % of the total, is somewhat similar to those observed in Figs. 3b, e. The residual transverse intensity is not uniform even below 500 Hz ^{15}N off-resonance frequency, because of the ^1H pulse imperfection, and increases significantly at >500 Hz. Importantly, the profiles of the two ^1H–^{15}N J-coupled ^{15}N peaks differ relative to each other when ^1H off-resonance is significant (circles and triangles in Fig. 8a, b). Since one of the X or Y components remains as an antiphase component, even after detection of the ^{15}N 90° pulse, the observed intensity difference likely contributes to the $R_1^{(1)}$–$R_1^{(2)}$. The magnitude of the transverse magnetization of these two J-coupled ^{15}N peaks becomes smaller at 400 Hz ^1H off-resonance frequency (Fig. 8c, d).

Taken together, the simulation suggests that the difference in the signal intensities between the two ^1H–^{15}N J-coupled ^{15}N peaks occurs due to imperfection of the ^1H 180° pulses and is enhanced by the ^1H off-resonance frequency. The simulation also suggests that the error affects the residual ^{15}N transverse magnetization, resulting in ^{15}N off-resonance frequency dependency.

Optimization of ^{15}N R_1 experiments

At the high magnetic fields required for NMR studies of large proteins in solution, i.e., >800 MHz, it must be kept in mind that spin relaxation behavior significantly differs from that at lower magnetic field strength. The ratio $R_1^{(1)}$:$R_1^{(2)}$ becomes large as the field increase, making it more difficult to suppress the DD-CSA cross correlation effect: the relative magnitude of the CSA relaxation rate term, $(2/15)\omega_N^2\Delta\sigma_N^2$, against the dipolar term, $(1/10)\hbar^2\gamma_H^2\gamma_N^2/r_{NH}^6$, is 36 % at a 600 MHz instrument but increases to 81 % at a 900 MHz instrument. Here, $\Delta\sigma_N$ is the chemical shift anisotropy of ^{15}N nuclei, and γ_N and γ_H are gyromagnetic ratios of ^1H and ^{15}N, respectively. In addition, due to instrument limitations, the pulse power applied at 900 MHz is not significantly larger than at 600 MHz, therefore the effective B_1 field strength for off-resonance signals is lower at the higher field. The impact of the experimental parameters on the acquired relaxation data becomes significant (Figures S2 and S3). Actual DD-CSA cancellation efficiency also depends on the protein sample conditions, such as molecular tumbling, internal motion, and ^1H spin-flip effects.

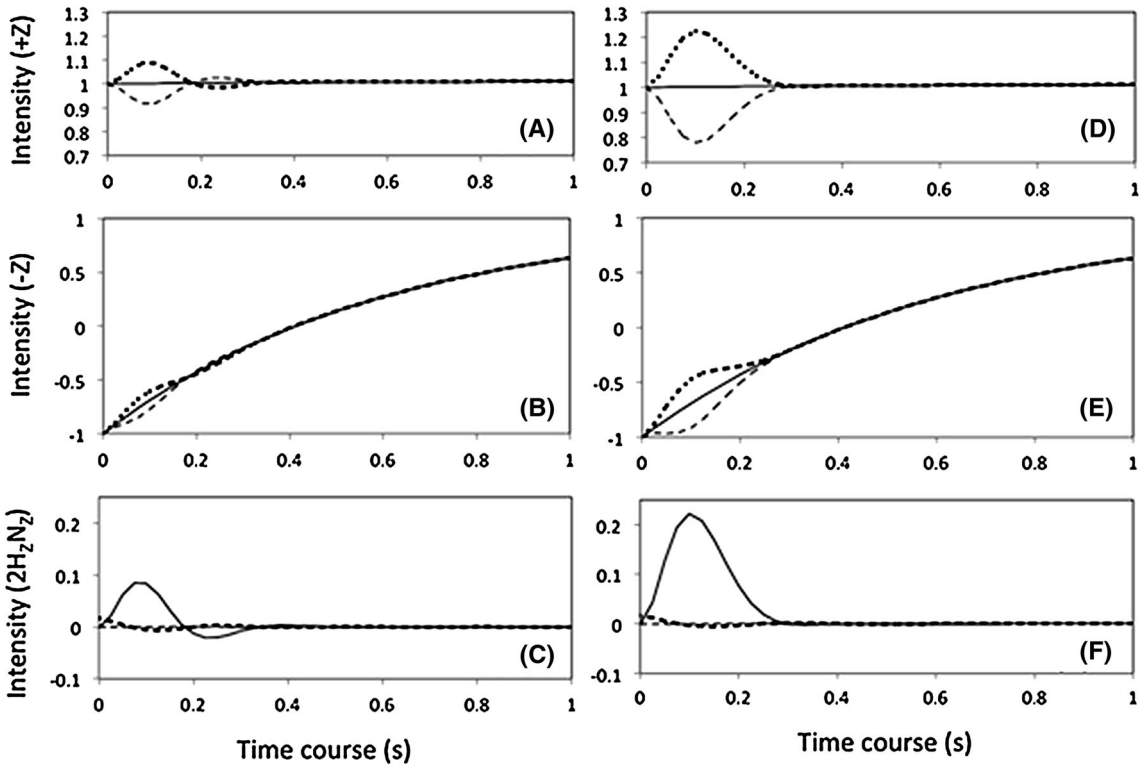

Fig. 7 Simulated time course of the longitudinal relaxation of the two components of the ^{1}H–^{15}N J-coupled ^{15}N resonance (*dashed lines*) and the average of the two (*solid line*), at every 4Δ interval in Fig. 1, for individual phases of the Freeman-Hill phase cycle, i.e., (*top panels*) starting from +Z and (*middle panels*) starting from –Z (Freeman and Hill 1971). ^{1}H off-resonance frequency was assumed to be **a**–**c** 3,000 Hz and **d**–**f** 400 Hz (3.3 and 0.44 ppm at 900 MHz, respectively). In **c** and **f** the time course of the $2N_ZH_Z$ term (*solid line*) and residual magnetization on X and Y axes (*dashed lines*) are shown. In the simulation, ^{15}N chemical shift was assumed to be 1,000 Hz (11 ppm at 91 MHz) away from the carrier position. During each 4Δ interval, two ^{1}H 180° pulses were assumed to be employed, as shown in in Fig. 1. See "Materials and methods" for other parameters

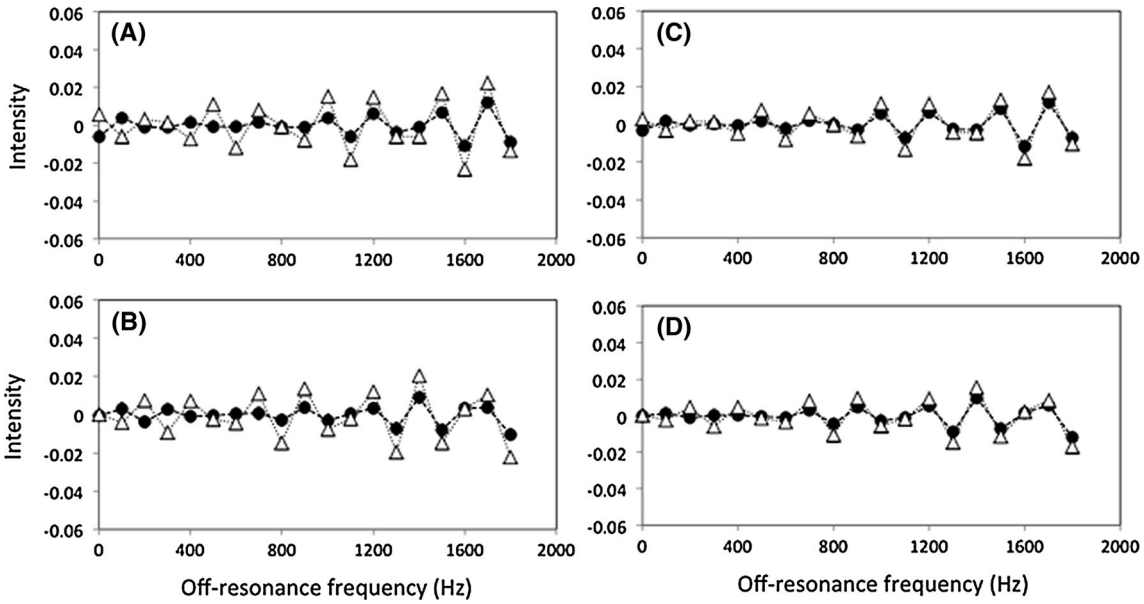

Fig. 8 Simulated residual intensity of the two components of the ^{1}H–^{15}N J-coupled ^{15}N resonance (one *circle*, and the other *triangle*) at $T_{R1} = 0.1$ s, **a**, **c** on the X-axis and **b**, **d** on the Y-axis, shown as a function of ^{15}N off-resonance frequency. During each 4Δ interval, two ^{1}H 180° pulses were employed, as shown in in Fig. 1, at **a**–**c** 3,000 Hz and **d**–**f** 400 Hz off-resonance frequencies for ^{1}H (which correspond to 3.3 and 0.44 ppm at 900 MHz, respectively)

Here, the above results show insufficient suppression of the DD-CSA cross correlation term and effects on the magnitude of $R_1^{(1)}$–$R_1^{(2)}$ for the deuterated ubiquitin. Simulation results suggest that the error is due to the imperfection of ^{1}H 180° pulses and the ^{1}H off-resonance frequency, and is further amplified by contamination of the ^{15}N transverse component. One could argue that additional pulsed-field gradient pulses may scramble the residual transverse component effect. However, achievement of the perfect inversion of amide protons together with perfect water-flip back pulses may be impractical. Instead, recording the ^{15}N R_1 delay points, by discarding the initial decay, is relatively simple. Based on the decay rates of the ^{15}N and $2N_ZH_Z$ terms, removal of $\sim$0.1 s may be needed to obtain more accurate R_1 values. In this case, $\sim$10 % loss of the initial intensity is noted.

Acknowledgments I thank Dennis Torchia and Teresa Brosenitsch for useful discussions and critical reading of the manuscript. This study was financially supported by National Science Foundation research grant MCB 0814905, National institutes of health 5P50GM082251-07, and University of Pittsburgh.

References

Allard P, Helgstrand M, Hard T (1998) The complete homogeneous master equation for a heteronuclear two-spin system in the basis of Cartesian product operators. J Magn Reson 134:7–16

Andrec M, Montelione GT, Levy RM (1999) Estimation of dynamic parameters from NMR relaxation data using the Lipari–Szabo model-free approach and Bayesian statistical methods. J Magn Reson 139:408–421

Boyd J, Hommel U, Campbell ID (1990) Influence of cross-correlation between dipolar and anisotropic chemical shift relaxation mechanisms upon longitudinal relaxation rates of 15 N in macromolecules. Chem Phys Lett 175:477–482

Bruschweiler R (2003) New approaches to the dynamic interpretation and prediction of NMR relaxation data from proteins. Curr Opin Struct Biol 13:175–183

Campbell AP, Spyracopoulos L, Irvin RT, Sykes BD (2000) Backbone dynamics of a bacterially expressed peptide from the receptor binding domain of Pseudomonas aeruginosa pilin strain PAK from heteronuclear 1H-15 N NMR spectroscopy. J Biomol NMR 17:239–255

Chen K, Tjandra N (2012) Water proton spin saturation affects measured protein backbone 15 N spin relaxation rates. J Magn Reson 213:151–157

Chen J, Brooks CLI, Wright PE (2004) Model-free analysis of protein dynamics: assessment of accuracy and model selection protocols based on molecular dynamics simulation. J Biomol NMR 29:243–257

Clore GM, Driscoll PC, Wingfield PT, Gronenborn AM (1990) Analysis of the backbone dynamics of interleukin-1 beta using two-dimensional inverse detected heteronuclear 15 N-1H NMR spectroscopy. Biochemistry 29:7387–7401

d'Auvergne EJ, Gooley PR (2003) The use of model selection in the model-free analysis of protein dynamics. J Biomol NMR 25:25–39

d'Auvergne EJ, Gooley PR (2006) Model-free model elimination: a new step in the model-free dynamic analysis of NMR relaxation data. J Biomol NMR 35:117–135

Dayie KT, Wagner G, Lefevre JF (1996) Theory and practice of nuclear spin relaxation in proteins. Ann Rev Phys Chem 47:243–282

Farrow NA, Muhandiram R, Singer AU, Pascal SM, Kay CM, Gish G, Shoelson SE, Pawson T, Forman-Kay JD, Kay LE (1994) Backbone dynamics of a free and phosphopeptide-complexed Src homology 2 domain studied by 15 N NMR relaxation. Biochemistry 33:5984–6003

Ferrage F, Piserchio A, Cowburn D, Ghose R (2008) On the measurement of 15 N-{1H} nuclear Overhauser effects. J Magn Reson 192:302–313

Ferrage F, Cowburn D, Ghose R (2009) Accurate sampling of high-frequency motions in proteins by steady-state (15)N-{(1)H} nuclear Overhauser effect measurements in the presence of cross-correlated relaxation. J Am Chem Soc 131:6048–6049

Freeman R, Hill HDW (1971) Fourier transform study of NMR spin–lattice relaxation by "progressive saturation". J Chem Phys 54:3367–3377

Fushman D, Cowburn D (2001) Nuclear magnetic resonance relaxation in determination of residue-specific N-15 chemical shift tensors in proteins in solution: protein dynamics, structure, and applications of transverse relaxation optimized spectroscopy. Methods Enzymol Nucl Magn Reson Biol Macromol Pt B 339:109–126

Fushman D, Tjandra N, Cowburn D (1999) An approach to direct determination of protein dynamics from N-15 NMR relaxation at multiple fields, independent of variable N-15 chemical shift anisotropy and chemical exchange contributions. J Am Chem Soc 121:8577–8582

Goldman M (1984) Interference effects in the relaxation of a pair of unlike spin-1/2 nuclei. J Magn Reson 60:437–452

Gong Q, Ishima R (2007) 15 N-{1H} NOE experiment at high magnetic field strengths. J Biomol NMR 37:147–157

Grzesiek S, Bax A (1993) The importance of not saturating H_2O in protein NMR—application to sensitivity enhancement and Noe measurements. J Am Chem Soc 115:12593

Idiyatullin D, Daragan VA, Mayo KH (2003) (NH)-N-15 backbone dynamics of protein GB1: comparison of order parameters and correlation times derived using various "model-free" approaches. J Phys Chem B 107:2602–2609

Igumenova TI, Frederick KK, Wand AJ (2006) Characterization of the fast dynamics of protein amino acid side chains using NMR relaxation in solution. Chem Rev 106:1672–1699

Ishima R, Torchia DA (2000) Protein dynamics from NMR. Nat Struct Biol 7:740–743

Jarymowycz VA, Stone MJ (2006) Fast time scale dynamics of protein backbones: NMR relaxation methods, applications, and functional consequences. Chem Rev 106:1624–1671

Jones JA (1997) Optimal sampling strategies for the measurement of relaxation times in proteins. J Magn Reson 126:283–286

Jones JA, Hodgkinson P, Barker AL, Hore PJ (1996) Optimal sampling strategies for the measurement of spin–spin relaxation times. J Magn Reson, Ser B 113:25–34

Kay LE (2005) NMR studies of protein structure and dynamics. J Magn Reson 173:193–207

Kay LE, Torchia DA, Bax A (1989) Backbone dynamics of proteins as studied by nitrogen-15 inverse detected heteronuclear NMR spectroscopy: application to staphylococcal nuclease. Biochemistry 28:8972–8979

Kay LE, Nicholson LK, Delaglio F, Bax A, Torchia DA (1992) Pulse sequences for removal of the effects of cross correlation between dipolar and chemical-shift anisotropy relaxation mechanisms on the measurement of heteronuclear T1 and T2 values in proteins. J Magn Reson 97:359–375

Korchuganov DS, Gagnidze IE, Tkach EN, Schulga AA, Kirpichnikov MP, Arseniev AS (2004) Determination of protein rotational correlation time from NMR relaxation data at various solvent viscosities. J Biomol NMR 30:431–442

Korzhnev DM, Skrynnikov NR, Millet O, Torchia DA, Kay LE (2002) An NMR experiment for the accurate measurement of heteronuclear spin-lock relaxation rates. J Am Chem Soc 124:10743–10753

Kroenke CD, Loria JP, Lee LK, Rance M, Palmer AG (1998) Longitudinal and transverse H-1-N-15 dipolar N-15 chemical shift anisotropy relaxation interference: unambiguous determination of rotational diffusion tensors and chemical exchange effects in biological macromolecules. J Am Chem Soc 120:7905–7915

Lee AL, Wand AJ (1999) Assessing potential bias in the determination of rotational correlations times of proteins by NMR. J Biomol NMR 13:101–112

Lee LK, Rance M, Chazin WJ, Palmer AG 3rd (1997) Rotational diffusion anisotropy of proteins from simultaneous analysis of 15 N and 13C alpha nuclear spin relaxation. J Biomol NMR 9:287–298

Lipari G, Szabo A (1982a) Model-free approach to the interpretation of nuclear magnetic resonance relaxation in macromolecules. 1. Theory and range of validity. J Am Chem Soc 104:4546–4559

Lipari G, Szabo A (1982b) Model-free approach to the interpretation of nuclear magnetic resonance relaxation in macromolecules. 2. Analysis of experimental results. J Am Chem Soc 104:4559–4570

Mandel AM, Akke M, Palmer AG 3rd (1995) Backbone dynamics of *Escherichia Coli* ribonuclease Hi—correlations with structure and function in an active enzyme. J Mol Biol 246:144–163

Massi F, Johnson E, Wang C, Rance M, Palmer AG 3rd (2004) NMR R1 rho rotating-frame relaxation with weak radio frequency fields. J Am Chem Soc 126:2247–2256

Myint W, Gong Q, Ishima R (2009) Practical aspects of 15 N CPMG transverse relaxation experiments for proteins in solution. Concepts Magn Reson 34A:63–75

Nicholson LK, Kay LE, Baldisseri DM, Arango J, Young PR, Bax A, Torchia DA (1992) Dynamics of methyl groups in proteins as studied by proton-detected 13C NMR spectroscopy. Application to the leucine residues of Staphylococcal nuclease. Biochemistry 31:5253–5263

Nirmala NR, Wagner G (1988) Measurement of C-13 relaxation-times in proteins by two-dimensional heteronuclear H1-C-13 correlation spectroscopy. J Am Chem Soc 110:7557–7558

Orekhov VY, Pervushin KV, Arseniev AS (1994) Backbone dynamics of (1-71) bacterioopsin studied by two-dimensional 1H-15 N NMR spectroscopy. Eur J Biochem 219:887–896

Palmer AG 3rd (2001) NMR probes of molecular dynamics: overview and comparison with other. Annu Rev Biophys Biomol Struct 30:129–155

Palmer AG, Rance M, Wright PE (1991) Intramolecular motions of a zinc finger DNA-binding domain from Xfin characterized by proton-detected natural abundance 13C Heteronuclear NMR spectroscopy. J Am Chems Soc 113:4371–4380

Palmer AG, Skelton NJ, Chazin WJ, Wright PE, Rance M (1992) Suppression of the effects of cross-correlation between dipolar and anisotropic chemical-shift relaxation mechanisms in the measurement of spin–spin relaxation rates. Mol Phys 75:699–711

Pelupessy P, Ravindranathan S, Bodenhausen G (2003) Correlated motions of successive amide N–H bonds in proteins. J Biomol NMR 25:265–280

Peng JW, Thanabal V, Wagner G (1991) Improved accuracy of heteronuclear transverse relaxation time measurements in macromolecules. Elimination of antiphase contributions. J Magn Reson 95:421–427

Redfield C (2004) Using nuclear magnetic resonance spectroscopy to study molten globule states of proteins. Methods Mol Biol 34:121–132

Renner C, Schleicher M, Moroder L, Holak TA (2002) Practical aspects of the 2D N-15-{H-1}-NOE experiment. J Biomol NMR 23:23–33

Schneider DM, Dellwo MJ, Wand AJ (1992) Fast internal main-chain dynamics of human ubiquitin. Biochemistry 31:3645–3652

Skelton NJ, Palmer AG, Akke M, Kordel J, Rance M, Chazin WJ (1993) Practical aspects of 2-dimensional proton-detected N-15 spin relaxation measurements. J Magn Reson, Ser B 102:253–264

Spyracopoulos L (2006) A suite of mathematica notebooks for the analysis of protein main chain (15)N NMR relaxation data. J Biomol NMR 36:215–224

Tjandra N, Kuboniwa H, Ren H, Bax A (1995) Rotational dynamics of calcium-free calmodulin studied by 15 N-NMR relaxation measurements. Eur Biochem 230:1014–1024